2008 IEEE International Conference on
Robotics and Automation
Pasadena, CA, USA, May 19-23, 2008

A Novel Method for Hydrothermal Vents Prospecting Using an Autonomous Underwater Robot

Gabriele Ferri [1,2] , Michael V. Jakuba [3] , Dana R. Yoerger [3]

e-mail : g.ferri@imtlucca.it

[1] *School of Biorobotic Engineering*
IMT Lucca Institute for Advanced Studies
Piazza S. Ponziano 6, 55100 Lucca, Italy

[2] *CRIM Laboratory*
Scuola Superiore Sant'Anna
Viale Rinaldo Piaggio 34, 56025 Pontedera (Pisa), Italy

[3] *Deep Submergence Laboratory*
Woods Hole Oceanographic Institution
Woods Hole, MA 02543, USA

Abstract – **In this paper we address the problem of localizing active hydrothermal vents on the seafloor using an autonomous underwater vehicle (AUV). Woods Hole Oceanographic Institution's Autonomous Benthic Explorer (ABE) (see Fig.1) AUV has been successfully used in several hydrothermal vents prospecting missions. Recently, a three-stage nested approach [1] has been introduced. It consists in surveys at different altitudes to finally photograph the venting structures flying very close to the seafloor. In this paper, we introduce a new strategy for ABE's movement in surveys at higher altitude (phase-1): ABE moves along pre-designed tracklines sampling the seawater; when some conditions on collected data are encountered, it starts a spiral movement to fly over areas likely to contain active vent fields. Results of the proposed algorithm tested on data coming from previous ABE's missions are shown and assess the efficiency and reliability of the method.**

Index Terms **- trigger based methods, hydrothermal vents, chemical source localization.**

I. INTRODUCTION

THIS paper addresses the problem of localizing active hydrothermal vents using an autonomous underwater vehicle (AUV). Hydrothermal plumes are caused by thermal and chemical input from submarine hot spring systems into the oceans at mid-ocean ridges. Since the first discovery of hydrothermal vents in 1979 [2], these deep ocean phenomena have catalyzed an enormous interest in the scientific community for different reasons: the hydrothermal circulation of seawater through the oceanic crust influences many geological and oceanographic processes such as loss of heat from the earth, geochemical cycling of the elements, biogeochemistry of deep ocean waters, possibly general ocean circulation [3] and the biology of hydrothermal vents communities presents unique features [4].

The hot, chemically altered seawater is vented as a buoyant plume (BP) that rises from the seafloor entraining in a turbulent way the surrounding water [5]. During the ascent, the buoyancy of the plume, with continuing entrainment of denser fluids, begins to decrease [6]. At the moment of neutral buoyancy the momentum reaches a maximum. This remaining momentum implies an overshoot of the rising plume. When finally the zero momentum condition is reached, the plume sinks back to its level of neutral buoyancy and spreads laterally advected by the flow (mean, tidally forced and venting induced). This non-buoyant plume (NBP) presents a vertical thickness of O(100 m) [7]. The difference between the equilibrium height (when neutral buoyancy is reached) and the final height has been observed to be of O(100 m) [8]. The rise height of the plumes can reach 100-400 m in typical hydrographic settings [8]. Models predict, in a time averaged sense, that the plume, during its rising from the seafloor to the equilibrium height, has expanded laterally from few centimeters to 50-100 m [8].

Although hydrothermal plumes can be detected up to a distance of several kilometers away from the emitting vent field with standard in situ sensors [7] their characteristics make pinpointing vent sites themselves time-consuming and challenging.

Traditionally, towed assets are used to come into contact with hydrothermally altered waters and to constrain their depth. Once the depth of the hydrothermal plume is constrained, the use of an AUV appears to offer some advantages with respect to towed assets (AUVs are well suited for pre-planned surveys using sonars and in-situ chemical sensors [9]), in order to find the signature O(100 m) of the buoyant plume rising from the seafloor. Woods Hole Oceanographic Institution's Autonomous Benthic Explorer (ABE) [10] AUV (see Fig.1) has been successfully used in several hydrothermal vents prospecting missions [9], [11], [12].

Recently, a three-stage (see Fig. 2) nested survey method has been introduced in [1] with success. This methodology is composed by different surveys at three different altitudes: the first phase (Hydrographic mapping of non-buoyant plume) at an altitude of 200-400 m, the second phase (Hydrographic and multibeam bathymetric mapping) at an altitude of about 50 m, and the third one (Photo-mosaicking of individual vent fields) at an altitude of 3-5 m. During these phases, pre-designed tracklines are covered by ABE. The data collected by the robot during the surveys are studied once the robot is recovered and new surveys are designed. The aim of the methodology is to circumscribe areas likely to contain venting activity and finally to let ABE fly over them during phase-3 surveys to photo-mosaick the vent fields. Given that the ratio of time associated with inter-survey recovery, maintenance and deployment related to the time spent collecting data is roughly 2:1 [12], an automation in the procedure would improve the efficiency of the mission. Flying over areas likely to contain waters of nascent plumes rising from the seafloor collecting useful data would strongly improve the

efficiency in localizing vents. This is true, above all, during phase-1. This phase, in fact, presents certain additional difficulties: the water current is not always accurately measured by ABE due to the acoustic Doppler measurements failures caused by its altitude; the altitude implies the measured anomalies are lower in magnitude and present an increased spatial extent with respect to those encountered to lower heights; plumes present patches of anomalies interspersed with areas of unaltered background water [13]; the interceptions of water stems (typical radius O(100 m)) rising from the vents are rare due to the height and to the wide spaced used tracklines (usually spaced more than 200 m). In these conditions, the use of gradient ascent-based [14] and bio-mimetic methods [15] appears to be problematical. In this setting, the absence of a well defined gradient and the fact that high intensity anomalies caused by tidal currents may be found far away from the source imply gradient ascent-based methods are liable to wander or to get "stuck" near local maxima. Bio-mimetic schemes usually rely on measurement of wind/crossflow to trace the plume up to the source. In phase-1 surveys, the oscillatory tidal components and, in a minor way, the difficulties in having a precise measure of the flow can confound them. Bio-mimetic schemes, however, can be a robust alternative to dense tracklines at low altitudes if some tracers with residence time in water shorter than tidal timescales are considered. We have to underline that given the intrinsic multiple-sources nature of the problem the use of a purely reactive/behaviour based algorithm does not guarantee the needed exploration of the survey area because they offer no guidance on how to continue searching for other sources once a source has been found. These data-driven strategies can be used therefore in limited areas that are likely to contain some rising stems or used together with other methods providing a high-level guidance [16].

Despite these problems, some work has been done to move ABE autonomously. An algorithm taking autonomously decisions (new tracklines are added starting on possible interesting locations chosen after the tracers anomalies are propagated to the seafloor using a plume model and crossflow measurements), has been proposed and tested [9]. Even if the method is quite conservative it improved the efficiency of phase-3 dive: additional tracklines comprised only 5% of total mission time resulting in a 36% of high-value data collected showing how data-driven strategies can be effective [9]. However, the main obstacle to apply this method to phase-1 surveys is that it chooses the locations to investigate further once all the pre-planned tracklines have been covered. The large spatial extent of phase-1 would make it not feasible for ABE to come back on the chosen locations.

In this paper, we propose a movement strategy for ABE, called triggered spirals prospecting (TSP), particularly suited to phase-1 surveys aiming at mixing the robustness of pre-designed tracklines with the efficiency of reactive/bio-mimetic algorithms without relying on the often misleading and difficult to analyze information carried by the water current direction and intensity.

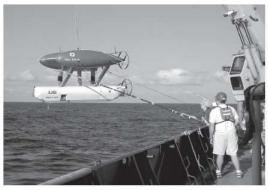

Fig.1.Recovery of Autonomous Benthic Explorer (ABE) vehicle.

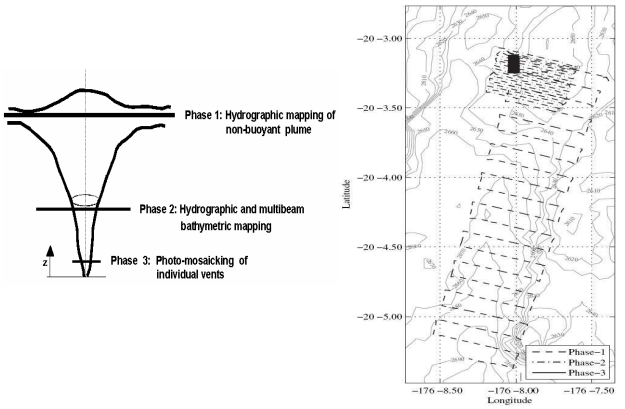

Fig.2. (Left) Schematic of a hydrothermal plume with the different altitudes for the three phase surveys. (Right) Three phases surveys tracklines covered by ABE at "Kilo Moana" vent field on Eastern Lau Spreading Center (20° 3´ S, 176° 12´ W) (Mid-Pacific Ridge).

II. TSP ALGORITHM

The objective of TSP is to enable ABE exploring further areas selected during a pre-planned path that are likely to contain nascent hydrothermal plumes: the additional collected information, in an off-line process, would be crucial for the scientific party to delimit regions likely to contain vent fields or to catalog some areas as likely empty. The new information may carry the evidence (water column vertical velocity anomalies [16]) of interceptions with buoyant plumes that unequivocally show the presence of nearby active vents.

The large spatial extent of phase-1 surveys imposes the strict constraint that the robot has to choose the locations to explore when it is not too far from them going on its pre-planned path. In this way, it can come back to the chosen locations without wasting too much mission time. This constrains TSP to trigger the movements basing only on past acquired information: we cannot complete the survey and then decide where to investigate (as the method proposed in [9] does given the smaller areas covered in phase-3). In our approach, ABE moves along pre-designed tracklines sampling the seawater. When an area containing clues of the presence of young hydrothermal waters is found out a spiral is triggered to acquire more information about that zone. The choice of a

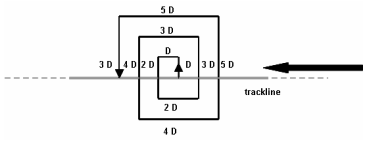

Fig. 3. Sketch of the pre-designed spiral movement. The only parameter changing the spiral is the basic spiral length *D*.

spiral movement is not critical for the algorithm, however it is an effective way of exploring an area and can be used in the future to propagate successive spirals like in the method proposed in [17]. The spiral arms length, shape and orientation are pre-designed (see Fig.3).

2.1. Tracers anomalies for nearby nascent plumes

In our case, we need tracers that present two features: they have to be reliable clues of nearby nascent hydrothermal plumes (not exclusively buoyant) and their anomalies with respect to background waters have to be computable in real-time. In recent missions the following anomalies were considered [16]: optical backscattering, potential temperature, vertical velocity anomalies and Eh anomalies. The first three anomalies are either related to NBP instead of BP or are not computable without the whole survey dataset (the low signal to noise ratio makes it difficult to have reliable real time computations). The last one, instead, presents the features we are looking for. We will consider only Eh anomalies as a trigger signal for spiral movements.

Reduction-oxidation (redox) potential (Eh) is a measure of the capability of chemical species in water to oxidate (positive Eh) or to reduce (negative Eh). The Eh potential has been measured by ABE using a sensor developed by Dr. Ko-ichi Nakamura (AIST, Tsukuba, Japan) and has showed a good tracer to detect nascent hydrothermal fluid. The nascent rising plume contains in fact reducing chemicals that are rapidly oxidized as the plume matures [18]. A low value of Eh, therefore, is a distinctive feature of young hydrothermal plumes. The Eh sensor has a complicate response characterized by a fast onset and a slow recovery time. Ongoing work by the instrument's inventor suggests that the magnitude of the differentiated Eh (dEh/dt) is strongly correlated with the chemicals typically present in young hydrothermal plumes [19]: steeply decreasing Eh signal appears to be a reliable sign of the interception of the younger part of hydrothermal plumes (not exclusively buoyant plumes). The instrument presents a relatively flat response in not altered water allowing to compute a background in real-time. In our experience, Eh anomalies are characterized by anomalously dEh/dt signal low values and by a relatively significant variance in dEh/dt values in a small number of samples (this is evident from Fig.4). The first step to declare Eh anomalies is to find a way of quantifying what our experience suggests. We consider the median absolute deviation (MAD) as a measure of variability of the dEh/dt signal in an interval. MAD is defined as the median absolute deviation from the median,

$$MAD(x)=med|x-med(x)| \quad (1)$$

where x is a data vector and *med* is the median operator.

To process Eh data during the survey we compute MADs on fixed temporal window of dEh/dt as the data are being collected by ABE: Eh signal acquired from the sensor is first low pass filtered and then a numerical derivative is computed; then, every N samples, a MAD is computed on dEh/dt signal (N is chosen to create a new window roughly every 50 s). As a result, we produce for every temporal window i one MAD_i. We have now a number (MAD_i) that represents a measurement of the variability of dEh/dt in each N-long samples temporal window. A high MAD_i means the temporal window i presents strong variations in dEh/dt signal showing that the robot is crossing waters likely altered by nascent hydrothermal waters. A method to declare a MAD_i as an anomaly has to be specified.

2.1.1. Background creation and anomaly detection

We approach the problem of anomalies declaration (or simply detections) as a problem of outliers detection on computed MAD_i. The idea is to consider as outliers MAD_i whose distance from the median of a reference data vector is greater than a threshold. The reference vector has to contain MAD_i computed in an area where the water is not altered by hydrothermal vents. We considered a reference vector fixed in time during the survey because we assume no valuable drifts in Eh signal measurements. To calculate the background, when the robot is not in hydrothermally altered waters (during ABE's descent), we compute a number N_B of MAD_i. On the computed MAD_i we calculate the median (MED_B) and the MAD (MAD_B), that is MED_B = med(MAD_i) and MAD_B = MAD(MAD_i) in both cases for all i in the descent. During the survey, a new computed MAD_i is considered as a detection if:

$$(MAD_i - MED_B) \geq c \cdot 1.4286 \cdot MAD_B \quad (2)$$

where c is a constant derived from analysis of previous data (c is equal to 9 in all our trials) and 1.4286 is a normalization value usually used to make the MAD an unbiased estimate of the standard deviation for Gaussian data [20]. MAD has been proved to be a robust measure for data variability in outlier detection problems [20]. In our trials, we considered N_B to compute the background on a temporal window of 50 minutes: a trade-off between assuring a less variable MAD_B (wider windows) and avoiding the inclusion in the computation of altered areas potentially encountered towards the end of the descent. Finally, we exclude from anomalies declaration MAD_i originated from windows with always positive dEh/dt signal (these windows derive from periods of slow recovery of Eh sensor with high variability of the signal).

The MAD_i declared as detections are related to periods (see Fig.4) (and areas) of the survey characterized by an increased variability of dEh/dt. Methods to choose areas with the highest anomalies (highest values of MAD_i) of the survey have to be introduced (next two sections).

2.2. Patches and clusters creation

The computed detections are grouped using a two-layered procedure: first they are aggregated into groups of detections (called patches), and then the patches are grouped into clusters. The best patch (we have still to define what "best" patch means) of one cluster triggers a spiral movement.

Patches creation: a patch is started once a detection is encountered. Next MAD_i declared as detections are assigned to that patch until it is finished. The patch is considered finished when there are no detections in consecutive *DP* MAD_i. *DP* is chosen equal to 6 to let a time of about 5 m without detections cause the end of the patch. The patches are stored in memory, each one with its centroid chosen as the location of the highest MAD_i belonging to the patch (the highest MAD_i is called the patch value (*PV*)). The location of a MAD_i is chosen as the position of the middle dEh/dt sample in the *N*-long data vector from which the MAD_i is computed. When a patch is closed, its *PV* is compared with a trigger threshold ($\eta_{trigger}$): if it is greater, that is, if

$$PV \geq \eta_{trigger} \quad (3)$$

a cluster is started. The trigger threshold $\eta_{trigger}$ is the threshold discriminating if a patch of anomalies is able to trigger a spiral movement.

Clusters creation: when the condition (3) is verified for one patch, a cluster is started and the patch is added to the new cluster. Next created patches for which (3) is true are added to the current cluster. The cluster is closed after a distance of *DC* meters from the centroid of the first patch of the cluster has been covered; if one patch is being created after DC meters the cluster is closed at the end of that patch. The *DC* value is a tunable parameter and represents how near we permit different spirals can be triggered. In our trials we chose a *DC* value constituting about the 2.5% of the total length of the tracklines covered by ABE. Once a cluster is closed, the patch in the cluster with the highest *PV* (we consider this as the merit value for patches) is chosen and a spiral movement starting from the centroid of that patch is triggered.

The second method aiming at selecting only the highest *PV* patches relies on how the trigger threshold is dynamically modified during the survey.

2.3. Trigger threshold

Phase-1 dives present different dEh/dt profiles: some present many areas with high intensity perturbations, others present low intensity anomalies. A static trigger threshold is not therefore the best solution: a too low one can cause too many spirals thereby consuming the batteries before something interesting is encountered; a too high one can trigger rarely losing possible interesting areas. We approach this problem using an adaptation mechanism for the threshold. At the beginning of the survey $\eta_{trigger}$ is fixed to the value $\eta_{triggerB}$. The unit of measure of $\eta_{trigger}$ is the normalized MAD_B . This avoids the difficult problem to provide an absolute value for the threshold. $\eta_{triggerB}$ is chosen equal to 180 basing on our experience on phase-1 collected data. The adapting mechanism depends on a number of suggested spirals (*SS*) and on how the survey is progressing. The number of suggested spirals is a design parameter and is an indication of how many spirals ABE is able to start.

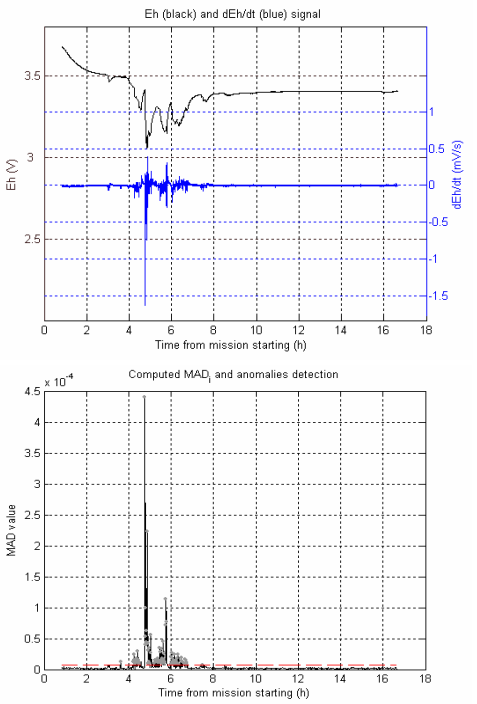

Fig.4. Process of MAD_i creation starting from Eh measurements coming from a phase-1 at "Kilo Moana" vent field on Eastern Lau Spreading Center (20° 3´ S, 176° 12´ W) (Mid-Pacific Ridge) are reported. At the top Eh signal (black) and the filtered and derivated Eh signal (blue) are reported. Finally, at the bottom, the computed MAD_i are shown with grey dots marking the detected anomalies. The dashed line represents the threshold above which a MAD_i is considered a detection. From the figure it is clearly visible how high MAD_i are correlated with portions of dEh/dt signal characterized by high variability.

However, it is not a constraining parameter in the sense that TSP allows that more or less spirals than *SS* can be started even if it can be considered as a sort of maximum number of allowed spirals. In all our trials we considered a value for *SS* equal to 5.

The idea of the adaptation mechanism basing on the ongoing status of the survey is essentially the following: if the percentage of triggered spirals with respect to the suggested ones is lower than the percentage of covered tracklines then the threshold is lowered, otherwise it is increased. The threshold modifications depend on so far created *PV* to try to modify the threshold in a way suitable to the conditions encountered during the actual dive. The algorithm for adapting the threshold is run whenever a new patch is closed. The adaptation mechanism is shown in Table I.

III. RESULTS WITH DATA COMING FROM ABE'S PREVIOUS SURVEYS

TSP was tested using data collected by ABE in previous phase-1 surveys. It was tested on 7 datasets of different dives. The values of the used parameters have been presented in previous sections. The only remaining parameter to be specified is the basic spiral length: in all the trials except one the basic spiral length *D* was 55 m. In one trial, given the wide spaced tracklines, we considered *D* equal to 150 m. The algorithm (implemented in Matlab from The MathWorks, Inc.) acquires raw Eh signal

Table I. Algorithm for adaptive threshold.

If *%Spirals ≤ %Tracklines* *// $\eta_{trigger}$ has to be lowered*
LowThr=median(Non_hit_patches(PV_i))
$\eta_{trigger}$ *=max($\eta_{triggerB}$ x (1-%Tracklines)+LowThr x K x %Tracklines, $\eta_{triggerMin}$)*
$\eta_{trigger}$*=min($\eta_{trigger}$, $\eta_{triggerB}$) //for the rare case of $\eta_{trigger}$> $\eta_{triggerB}$*
else *// $\eta_{trigger}$ has to be raised*
RaiseThr=median(Patches(PV_i))
$\eta_{trigger}$*=max($\eta_{triggerB}$ x (1-%Tracklines)+RaiseThr x K x %Tracklines, $\eta_{triggerB}$)*

%Spirals *is the number of done spirals divided by the number of suggested spirals;* ***%Tracklines*** *is the covered distance of tracklines divided by the scheduled total length of tracklines;* ***Non_hit_patches*** *is a function that selects among all the created patches only PV of patches that were not able to trigger a spiral;* ***Patches*** *selects the PV of all the created patches;* ***K*** *is a weighting constant equal to 2 and* $\eta_{triggerMin}$ *is a minimum threshold value that has been fixed to 100.*

recorded by ABE during the mission, the positions of the robot and computes the robot trajectory.

We discuss in detail the results for one dataset from a site at Southern Mid-Atlantic Ridge (SMAR) (4° 54´ S, 12° 28´ W) (see Fig.5). In this survey we used a spiral length of 150 m given the tracklines are 1 km spaced. Even if the tracklines spacing is very wide, the MAD_i show clearly three different regions of anomalies. In all three cases a spiral is started allowing the robot to fly over or very near vent fields (see Fig.5): all three perturbations revealed to be related with nearby buoyant plumes. Other lower Eh perturbations to the north are ignored by the algorithm. The three highest intensity areas are explored.

To investigate the efficiency of the method we analyze the results from the 7 available surveys quantifying how much the triggered spirals are related to nearby known hydrothermal activities. To do this, we group the triggered spirals in three different categories:

- spirals with confirmed nearby vents (active vents have been confirmed using photos taken by ABE in near bottom surveys): this category includes spiral movements presenting an arm passing at less than 150 m from a vent (100 m is the order of magnitude of a buoyant stem. So passing at that distance from a vent strongly increases the likelihood to intercept the buoyant plume). These movements are considered the best ones generated by TSP;
- spirals with likely nearby vents: it groups movements in areas that even if they have not been explored with phase-3 dives, they present from an off-line analysis clues of nearby vents activity or however they present the highest Eh perturbations of the survey;
- other spirals: spirals in this category are considered avoidable if the energetic constraints do not allow to cover all the trajectories suggested by TSP.

In Table II we report the results using TSP with the available previously collected data. To investigate how the adapting threshold mechanism works we report either the results with the use of adapting mechanism or with a fixed trigger threshold ($\eta_{trigger}$=180). The results show the efficiency of TSP approach. The high percentage of spirals belonging to the first two categories together with the limited total number of triggered spirals (the average

Table II. Results using TSP with the threshold adapting mechanism and with a fixed trigger threshold. TSP has been used on 7 datasets coming from previous ABE's phase-1 dives.

	TSP with threshold adapting mechanism	**TSP with fixed threshold**
# spirals with confirmed nearby vents	11 (61.1 %)	9 (56.3 %)
# spirals with likely nearby vents	5 (27.7 %)	4 (25 %)
# other spirals	2 (11.1 %)	3 (18.8 %)
# missed venting areas	2 (15.4 %)	4 (30.8 %)
# triggered spirals	total=18, μ=2.57, σ=1.4	total=16, μ=2.29, σ=1.67

is well under the suggested number of spirals (5)) assesses the efficiency of TSP in triggering spirals at interesting locations and in a not too large number. The suggested number of spirals (5) was reached only in one trial. In that trial, particularly diffused Eh perturbations triggered 5 spirals for TSP with the adaptation mechanism and 6 spirals for that without adaptation. The analysis of the differences between the two versions of TSP shows that using an adapting threshold offers more robustness: the adaptive TSP presents a higher percentage of triggers in the first two categories and, more importantly, the fixed threshold TSP missed two more venting areas. We consider "to miss" a venting area if the robot, during a spiral movement, does not pass at a distance shorter than 150 m from the area.

However, as for every method using some thresholds to make decisions, one delicate issue is how to choose the

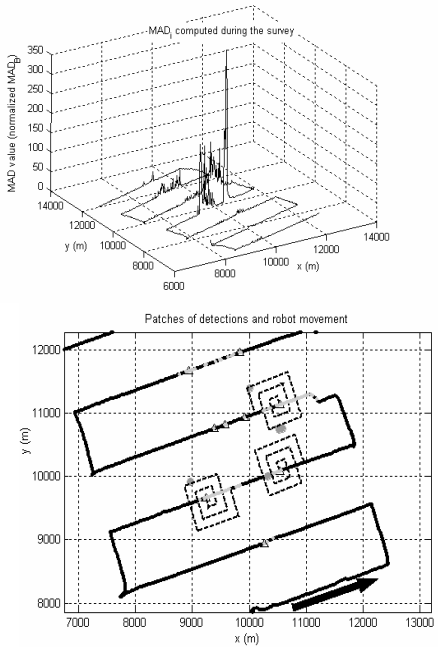

Fig. 5. 3D image of created MAD_i (top) and trajectory generated by TSP. (bottom). Robot trajectory shows three triggered spirals, one for each of the three regions of highest anomaly. The triggered movements sweep areas containing all the vents (grey circles) currently known in the site. Dots along the tracklines represent the locations of created MAD_i: black dots are non-detections, grey ones are the detections. Triangles mark the positions of patches centroids. Finally, the black arrow shows the direction of ABE's movement. The two plots are produced using TSP with data collected in a phase-1 dive at SMAR site (Southern Mid-Atlantic Ridge) (4° 54´ S, 12° 28´ W).

starting threshold. We chose it to be 180 times the normalized MAD_B basing on our experience from data from previous surveys. To investigate the robustness of the chosen threshold we ran also the program with two other trigger thresholds: 140 and 220. The three thresholds were used as the basic trigger threshold ($\eta_{triggerB}$) for the adapting mechanism and also as the fixed $\eta_{trigger}$ without the adapting mechanism. Results confirm the robustness of the adaptive threshold TSP: the number of spirals changed only in one survey not causing differences in the percentage of missed vents, while in the fixed threshold version the number of spirals changed from 19 ($\eta_{trigger}$=140) to 14 ($\eta_{trigger}$=220). In the first case, the percentage of missed venting areas (on the total number of known venting fields) was 23.1 %, in the second one was 38.5 %.

IV. Conclusions and Future Works

In this paper we address the problem of localizing hydrothermal vents using an AUV. We present a method to improve ABE's movements during phase-1 surveys. This phase appears to be the most difficult in the three stage nested strategy [1] used in recent ABE's missions. TSP aims at mixing the robustness of pre-designed tracklines with the efficiency of reactive/bio-mimetic algorithms without considering the often misleading and difficult to analyze information carried by the water current direction.

Our approach has been tested on 7 datasets collected during phase-1 dives. It proved to work well with a percentage of 88.8% of spirals triggered in very interesting areas. The effectiveness of threshold adapting has been investigated showing it improves TSP robustness to changes in starting threshold and it adapts the threshold to the ongoing survey. The number of triggered spirals was on average 2.57: it is an acceptable number thinking to the additional distance ABE has to cover during the spirals. The suggested spirals would have carried likely useful information to localize venting fields.

One trial, however, resulted in 5 spirals (6 spirals with the lower used basic threshold), a quite large number. This may happen in surveys with high intensity anomalies. Even if the improved autonomy of new generation AUVs will reduce this problem, we will work on possible solutions. A solution could be not using spirals of pre-designed length. After a spiral is triggered, if during the movement no high Eh perturbations are encountered, ABE could come back to move on the tracklines aborting the actual spiral. In this way it would have the possibility to trigger on all interesting areas, but continuing the movement only if relatively high Eh perturbations were found. In the future, TSP algorithm will be implemented on ABE and tested in phase-1 surveys for hydrothermal vents prospecting. The acquired data will be also useful to design the above described strategy.

References

[1] C.H. Langmuir et al., "Hydrothermal prospecting and petrological sampling in the Lau Basin: background data for the integrated study site", in *Eos. Trans. AGU*, volume 85, 2004. Fall Meet. Suppl., Abstract B13A-0189.

[2] J. Corliss et al., "Submarine thermal springs on the Galapagos Rift", *Science*, vol. 203, pp. 1073-1083, 1979.

[3] D. Kadko, J. Baross and J. Alt, "The magnitude and global implications of hydrothermal flux", in *Seafloor hydrothermal systems: physical, chemical, biological, and geological interaction*, American Geophysical Union, Geophysical Monograph 91, 1995, pp. 446-466.

[4] C.R. Fisher, "Toward an appreciation of hydrothermal-vent animals: their environment, physiological ecology, and tissue stable isotope values", in *Seafloor hydrothermal systems: physical, chemical, biological, and geological interaction*, American Geophysical Union, Geophysical Monograph 91, 1995, pp. 297-316.

[5] J.S. Turner, "Turbulent entrainment: the development of the entrainment assumption, and its application to geophysical flows", *Journal of Fluid Mechanics*, vol. 173, pp. 431-471, 1986.

[6] R.E. McDuff, "Physical dynamics of deep-sea hydrothermal plumes", in *Seafloor hydrothermal systems: physical, chemical, biological, and geological interaction*, American Geophysical Union, Geophysical Monograph 91, 1995, pp. 357-368.

[7] E.T. Baker, C.R. German, and H. Elderfield, "Hydrothermal plumes over spreading-center axes: global distributions and geological inferences", *Seafloor hydrothermal systems: chemical, biological, and geological interaction*, American Geophysical Union, Geophysical Monograph 91, 1995, pp. 47-71.

[8] K.G. Speer, and P.A. Rona, "A model of an Atlantic and Pacific hydrothermal plume", *Journal of Geophysical Research*, Vol. 94, No. C5, pp. 6213-6220, 1989.

[9] D.R. Yoerger et al., "Techniques for deep sea near bottom survey using an autonomous underwater robot", *International Journal of Robotics Research,* Volume 26, Issue 1, pp. 41-54, January 2007.

[10] D.R. Yoerger, A.M. Bradley, and B.B. Warren, "The Autonomous Benthic Explorer (ABE): an AUV optimized for deep seafloor studies", in *Proc. of the 7th International Symposium on Unmanned Untethered Submersible Technology (UUST91)*, Durham, NH, USA 1991, pp. 60-70.

[11] C.R. German et al., "New techniques for hydrothermal plume investigation by AUV", in *Geophysical Research Abstracts*, European Geosciences Union Vienna, Austria, volume 7, 2005.

[12] M. Jakuba et al., "Multiscale, multimodal AUV surveys for hydrothermal vent localization", in *Proc. of the 14th International Symposium on Unmanned Untethered Submersible Technology (UUST05),* Durham, NH, USA 2005.

[13] J.E. Lupton, "Hydrothermal plumes: near and far field" in *Seafloor hydrothermal systems: physical, chemical, biological, and geological interaction*, American Geophysical Union, Geophysical Monograph 91, 1995, pp. 317-346.

[14] E. Burian et al., "Gradient search with autonomous underwater vehicles using scalar measurements", in *Proc. AUV '96*, Monterey, CA, USA, 1996, pp. 86-98.

[15] W. Li et al., "Moth-inspired chemical plume tracing on an autonomous underwater vehicle", *IEEE Transactions on Robotics*, Vol.22, No. 2, pp: 292 – 307, 2006.

[16] M.V. Jakuba, "Stochastic mapping for chemical plume source localization with application to autonomous hydrothermal vent discovery", PhD Thesis, WHOI-MIT, 2007.

[17] G. Ferri et al., "A biologically-inspired algorithm for gas/odor source localization in an indoor environment with no strong airflow: first experimental results", *ICRA 2007, Workshop on Robotic Olfaction,* Rome, Italy, April 10-14, 2007 .

[18] K. Nakamura et al., "Chemical signals in rising buoyant plumes and tidally oscillating plumes at the Main Endeavour vent field, Juan de Fuca Ridge" in *Eos. Trans. AGU*, volume 81,Fall Meet. Suppl., 2000, Abstract OS52I-05.

[19] K. Nakamura, AIST, Tsukuba, Ibaraki, Japan. Personal communication, November 2006.

[20] P.H. Menold, R.K. Pearson, and F. Allgower, "Online outlier detection and removal", in *Proc. of the 7th Mediterranean Conference on Control and Automation (MED99)*, Haifa, Israel. 1999, pp. 1110-1133.